The 14th International Topical Meeting on Nuclear Reactor Thermal Hydraulics, NURETH-14
Toronto, Ontario, Canada, September 25-30, 2011

NURETH14-201

UNSTEADY HYDRAULIC CHARACTERISTICS IN PIPE WITH ELBOW UNDER HIGH REYNOLDS CONDITION

A. Ono[1], N. Kimura[1], H. Kamide[1] and A. Tobita[1]
[1] Japan Atomic Energy Agency,
Narita 4002, O-arai, Ibaraki, 311-1393, JAPAN

Abstract

In the design of Japan Sodium-cooled Fast Reactor (JSFR), coolant velocity is beyond 9 m/s in the primary hot leg pipe of 1.27 m diameter. The Reynolds number in the piping reaches 4.2×10^7. Moreover, a short-elbow (r/D=1.0, r: curvature radius, D: pipe diameter) is adopted in the hot leg pipe in order to achieve compact plant layout and reduce plant construction cost. Therefore, the flow-induced vibration (FIV) arising from the piping geometry may occur in the short-elbow pipe. The FIV is due to the excitation force which is caused by the pressure fluctuation on the wall. The pressure fluctuation on the pipe wall is closely related with the flow fluctuation. In this study, water experiments using two types of 1/8 scaled elbows with different curvature ratio, r/D=1.0 and 1.5 (short-elbow and long-elbow), were conducted in order to investigate the mechanism of velocity and pressure fluctuation in the elbow and its downstream. The experiments were carried out at $Re=5.4 \times 10^5$ conditions. Measurement of velocity fluctuation and pressure fluctuation in two types of elbows with different curvature revealed that behavior of separation region and the circumferential secondary flow affected the pressure fluctuation on the wall of the elbow greatly.

1. Introduction

A conceptual design study of advanced sodium-cooled fast reactor named JSFR has been conducted in the FaCT (Fast reactor Cycle Technology development) project in Japan [1-2]. Figure 1 show a schematic view of primary cooling system of JSFR. The main cooling system

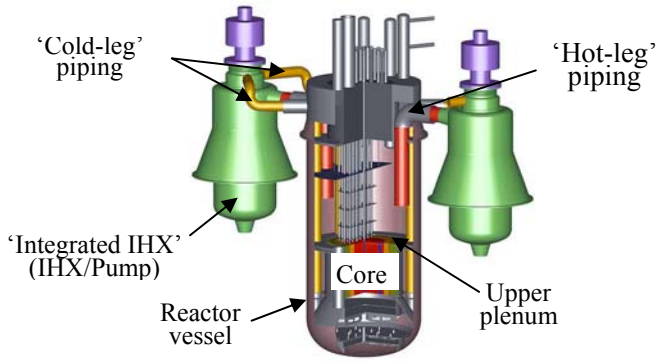

Figure 1 Schematic view of primary cooling system of the JSFR [1][2].

of JSFR consists of two loops in order to reduce the plant construction cost while the prototype fast reactor of Monju in Japan has three loops. In addition, the thermal output of JSFR is 3,600 MWt and much larger than that of Monju. Therefore, the sodium coolant flow velocity is beyond 9 m/s in the primary hot leg (H/L) of JSFR and the diameter of pipe is 1.27m. The maximum Reynolds number in the piping reaches 4.2×10^7. The H/L pipe having a 90 degree elbow with curvature ratio of r/D = 1.0, so-called 'short-elbow', is adopted to realize a compact layout of the primary cooling system. In sodium-cooled fast reactors, the system pressure is low and thermal stress is major component of load due to the large temperature difference of coolant in transition condition. Therefore, the thickness of pipe wall in the cooling system is thinner than that in light water reactors.

Under such a condition in the cooling system, flow-induced vibration (FIV) is concerned from a view point of the structural integrity of pipings. It is needed to investigate the probability that the H/L piping in JSFR is vibrated destructively under the operating condition. The flow structure in the 90 degree elbow with small curvature ratio is very complex and unsteady due to interaction between the flow separation and the secondary flow. In order to clarify the mechanism of FIV in the elbow with small curvature ratio, it is needed to understand about the structure and the characteristics of pressure fluctuation in the elbow.

Many studies on the fluid flow in the pipe with bend, elbow or curved duct have been conducted [3-5]. The most of them focused on pressure loss between inlet and outlet of elbow and time-averaged velocity profile from a view point of industrial applicability. Some studies were conducted on flow characteristics in the pipe with a 90^o bend or an elbow of circular cross-section.

Bovendeerd et al. [6] measured the velocity fields in a 90^o bend with curvature ratio, r/D=3, at Re=700 using Laser-Doppler Velocimetry (LDV). They chose oil and kerosene as a working fluid in order to match the refractive index of fluid to that of bend material (Perspex). They obtained the time-averaged axial and secondary velocities. Enayet et al. [7] measured the velocity and turbulent intensity fields in a 90^o bend pipe with r/D=2.8 at the Re=500, 1093 and 4.3×10^4 using LDV. Their working fluid was water and refractive index matching technique at the fluid-wall interface was not used. The displacement of the laser measurement volume due to refraction is allowed for simple geometrical conclusion. Sudou et al. [8] measured three components of mean and fluctuating velocities in a 90^o bend pipe with r/D=2 at $Re=6 \times 10^4$ using the hot wire probes. The working fluid was air.

The flow separation did not seem to occur in the experiments in above studies because of large elbow curvature ratio. In other words, the complex flow structure where the secondary flow interacted with the flow separation was not investigated. In JSFR, it is needed to clarify the mechanism of flow fluctuation inducing the FIV, when the flow separation occurs in the short-elbow geometry. Kawamura et al. [9] measured the velocity field and turbulence intensity field in a 90^o elbow with r/D=0.55, 1 and 2 at the $Re=5 \times 10^4$, 5×10^5 and 1×10^6 using LDV. They reported that the flow separation occurred in the case of r/D=0.55 and 1. They gave the important findings that normalized power spectrum of the velocity fluctuation was not affected by Reynolds number and elbow curvature ratio under their experimental condition. Shiraishi et al. [10-11] measured the pressure fluctuation and observed the flow regime in the pipe with

elbow of r/D=1 up to the Re=8.0x10^6. Although they concluded that the fluctuation pressure was generated by movement of the boundary of flow separation and reattachment region, their data of axial velocity profile in the elbow measured by LDV was limited at several positions and not enough to understand clearly the complex and unsteady flow field around the flow separation region.

In this study, water experiments using 1/8 scaled elbow were conducted in order to investigate the mechanism of velocity fluctuation and pressure fluctuation induced by interaction between flow separation and secondary flow. The unsteady velocity fields were measured using a high-speed Particle Image Velocimetry (PIV) and the pressure fluctuation on the wall was measured using the fiber optic pressure sensors. The elbow curvature ratio was chosen as an experimental parameter in order to investigate the influence of separation region on the velocity fluctuation in the elbow. The experiments were conducted using the two types elbows with different curvature ratio, r/D=1.0 (so-called 'short-elbow') and r/D=1.5 (so-called 'long-elbow').

2. Experiment

2.1 Experimental Set up

The experiments were conducted using water. Figure 2 shows the schematic of the test loop with the elbow. The details of the test loop were reported in a previous paper [12]. The inner diameter of pipe is 150 mm, which is 1/8 scaled model of the H/L pipe in JSFR. Two types of elbow, r/D=1.0 and 1.5, were used in the experiments. In general, the elbow with r/D=1.0 is called 'short-elbow' and the elbow with r/D=1.5 is called 'long-elbow'.

In this study, a high-speed PIV was adopted for measuring unsteady and complex velocity fields in the elbow and the pipe. It is difficult to measure the flow field in the round pipe by visualization method with high precision because the round pipe distorts the light at the wall. The seamless elbows with 3mm thickness were used to reduce the optical distortion of the captured image for PIV method. The optic distortion of these elbows was discussed in a previous paper [12] and we confirmed that the influence of refraction was small near the wall even though the elbow had the strong curvature wall. The fluorescing tracer particle and the optical sharp-edged band-cut filter were used in the PIV measurement to cut the reflection lights from the wall of pipes (halation). The ion-exchange resin (around 80 μm in diameter) dyed by

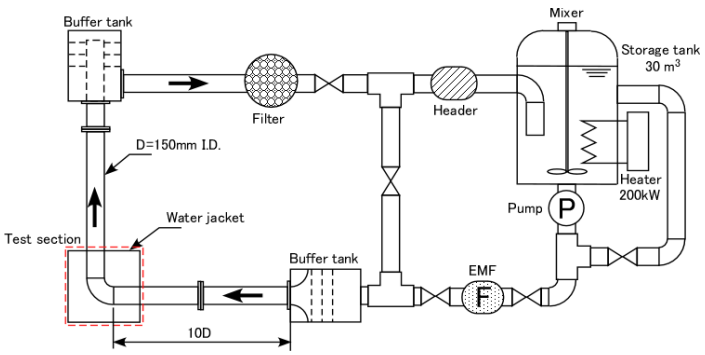

Figure 2 Schematic of the test loop.

Rhodamine-640 was used as fluorescent tracer particle.

In this experiment, the time intervals between two laser pulses, Δt, were set from 0.2ms to 1.5ms depending on the mean velocity of the captured area. The successive two frames were captured at sampling frequency of 200Hz. The total number of frames per one record was 6144, so the number of vector map obtained was 3072 with intervals of 5ms. Therefore, the total time length of record was 15.36s. The cross-correlation methods with sub-pixel accuracy were used for PIV data analysis. The spatial error of the correlation was nearly 0.2 pixel by using the sub-pixel method [13]. The estimated velocity measurement errors were less than 0.02m/s and 0.15m/s in the cases where the interval of laser emission were 1.5ms and 0.2 ms, respectively.

Figure 3 shows the schematic of the elbows for velocity measurement in this experiment. Here, 'elbow outlet' is defined as the termination point of curvature downstream side of the elbow. It is defined that the axial direction downstream the elbow is x-coordinate, the direction from the inside to outside of the elbow is y-coordinate and perpendicular direction to x and y is z-coordinate. The point on the inside wall at the elbow outlet is defined as the coordinate origin, x/D=0, y/D=0 and z/D=0, corresponding "O" in Fig.3.

In this experiment, the characteristics of pressure fluctuation on the pipe wall downstream of the elbow were measured using the fiber optic pressure sensors. The measurement system and the

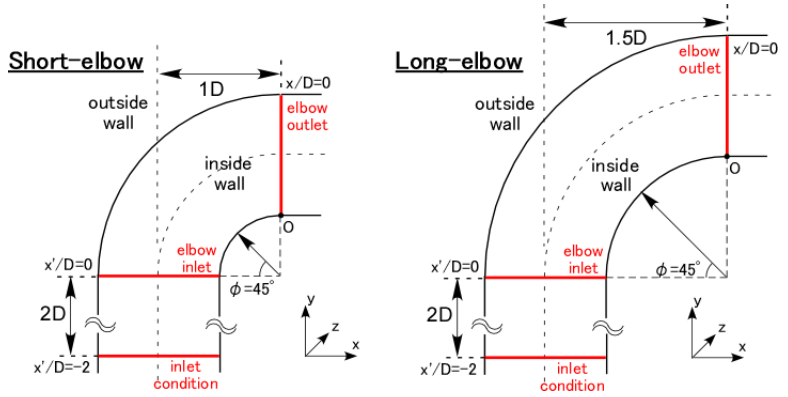

Figure 3 Schematic of the elbows for velocity measurement.

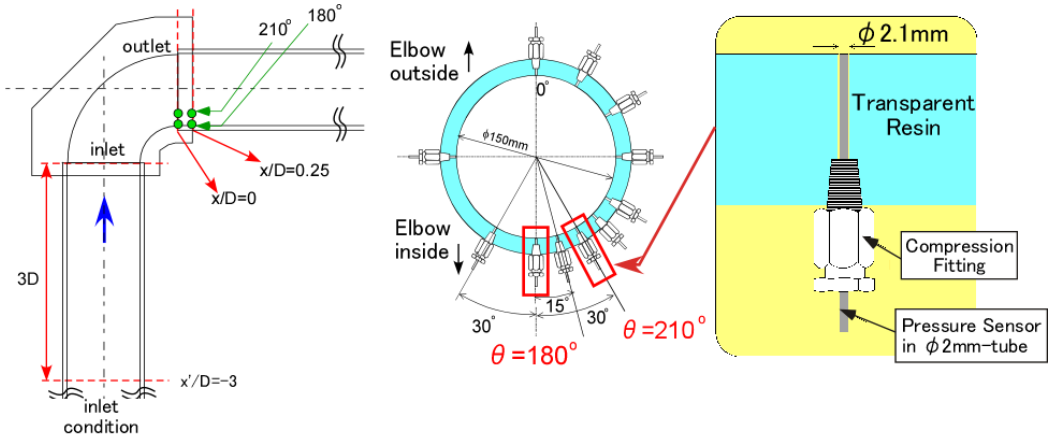

Figure 4 Schematic of the elbows for pressure measurement.

test section for measurement of pressure fluctuation were described in detail in [12]. The interval of data sampling was 1ms. The measurements for 100s were conducted three times to increase statistical accuracy. Figure 4 shows the positions of pressure measurements. Five sensors were set at '-3D-180°', '0D-180°', '0D-210°', '0.25D-180°' and '0.25D-210°'. '-3D-180°' was 3D upstream from elbow inlet for measuring inlet condition. The line '0.25D' was 0.25D downstream from the elbow outlet. Here, we defined that the position at circumferential angle of $\theta = 0^{o}$ was outside of the elbow and the position at circumferential angle of $\theta = 180^{o}$ was inside of the elbow.

2.2 Experimental Condition

Idelchik et al. [14] arranged the previous data of total resistance coefficients of bends and divided them into three regimes: the sub-critical ($Re<1x10^5$), the transition ($1x10^5<Re<4x10^5$) and post-critical ($4x10^5<Re$) regimes. Starting with very small value of the Reynolds number, the coefficients of total resistance of the bend tend to drop in the sub-critical regime. Following this, the coefficients decrease as Reynolds number increases in the transition regime, and take nearly constant values in post-critical regimes. Shiraishi et al. [10-11] measured the velocity profile in the 90° short-elbow up to $Re = 8x10^6$ in the post-critical regime by using LDV. They found that the flow pattern and the dimensionless velocity distribution in the elbow were independent of Reynolds number in a region of $4x10^5<Re<8x10^6$ in the post-critical regime. They explained the reason why the flow resistance coefficient was constant in the post-critical regime as follows; the starting point of separation was rigid at certain location on the wall in the post-critical regime. In other words, the separation formation was independent of Reynolds number up to at least $Re=8x10^6$.

Therefore, it is important to clarify the flow structure in post-critical region in order to predict the flow regime at $Re=4.2x10^7$ in JSFR. There were a few studies focused on the mechanism of the fluid fluctuation and pressure fluctuation at the high Reynolds number in the post-critical regime. In this study, in order to investigate the characteristics of flow structure in the post-critical regime, experiments were conducted at Reynolds number $Re=5.4x10^5$ in the post-critical regime. The experimental condition was under U_m=3 m/s of the cross-section averaged flow velocity and 28 °C of fluid temperature. The elbow curvature, r/D, was selected as the experimental parameter. The curvature ratios were r/D=1.0 and 1.5. The inlet condition was defined from axial velocity 2D upstream of the elbow inlet. The turbulent intensity was 2.5% at the center of cross-section against the mean velocity.

3. Result and Discussion

3.1 Flow structure in the elbow

Figure 5 shows the velocity fields of u_{xy} in the elbow and downstream pipe. The upper is the short-elbow and the lower is the long-elbow. The maximum velocity was 4.7m/s near the elbow inside wall at 30° from the elbow inlet in the short-elbow case and 3.8m/s near the elbow inside wall 40° from the elbow inlet in the long-elbow case. Therefore the pressure at that point

in the short-elbow should be lower than that in the long-elbow. It is that the negative pressure gradient along the inside wall in the short-elbow would be larger than that in the long-elbow.

Figure 6 shows the instantaneous velocity fields at the elbow outlet in the short-elbow (the red square in Fig.5) at two arbitrary time points, (a) and (b). In the short-elbow case, it was found that the flow separation occurred around the elbow outlet since we could easily identify the boundary between the higher velocity region and lower velocity region. In Fig.6-(a), the reverse flow was seen in the lower velocity region. The occurrence of flow separation was

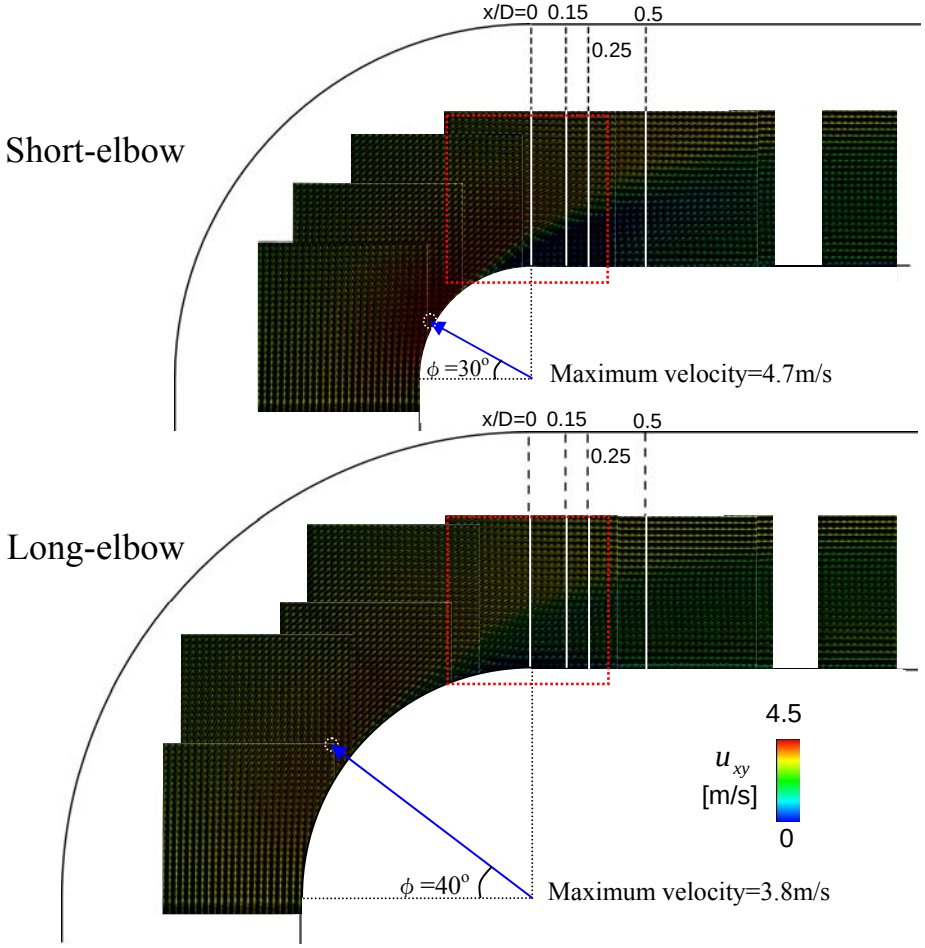

Figure 5 Velocity fields of u_{xy} in the elbow and the straight pipe.

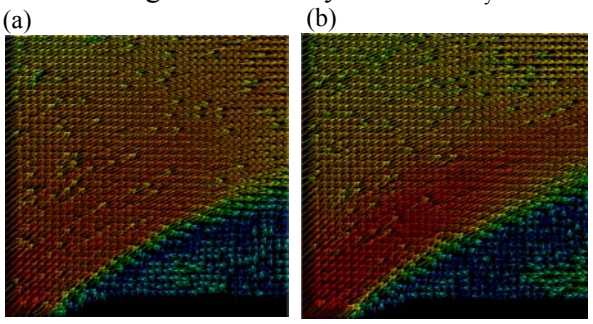

Figure 6 Instantaneous velocity fields in the short-elbow.

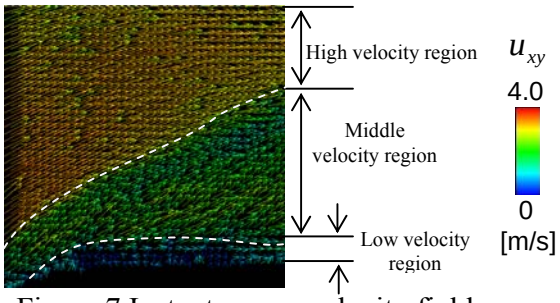

Figure 7 Instantaneous velocity fields in the long-elbow

caused by the large negative pressure gradient along the inside wall of the short-elbow. The high velocity flow in axial direction was sometimes observed in the separation region as shown in Fig.6-(b). The mechanism of this high velocity flow is explained later. Figure 7 shows the instantaneous velocity field at elbow outlet of the long-elbow (the red square in Fig.5). The flow structure in the long-elbow was different from that in the short-elbow. We can see the 'medium velocity region' between the higher velocity region of main flow and the separation region with lower velocity near the wall. The separation region formed in the long-elbow was much smaller than that in the short-elbow and its region was limited near the inside wall.

Figure 8 shows the instantaneous secondary flows in the cross-sections at x/D=0, 0.15, 0.25 and 0.5 in the short-elbow. In the cross-section of x/D=0, the large separation region was formed at θ =180° of the short-elbow constantly. At the cross-sections of x/D=0.15 and 0.25, the strong circumferential secondary flows were seen toward the elbow inside from both right and left sides. It was observed the strength of them varied with time. The strong secondary flows

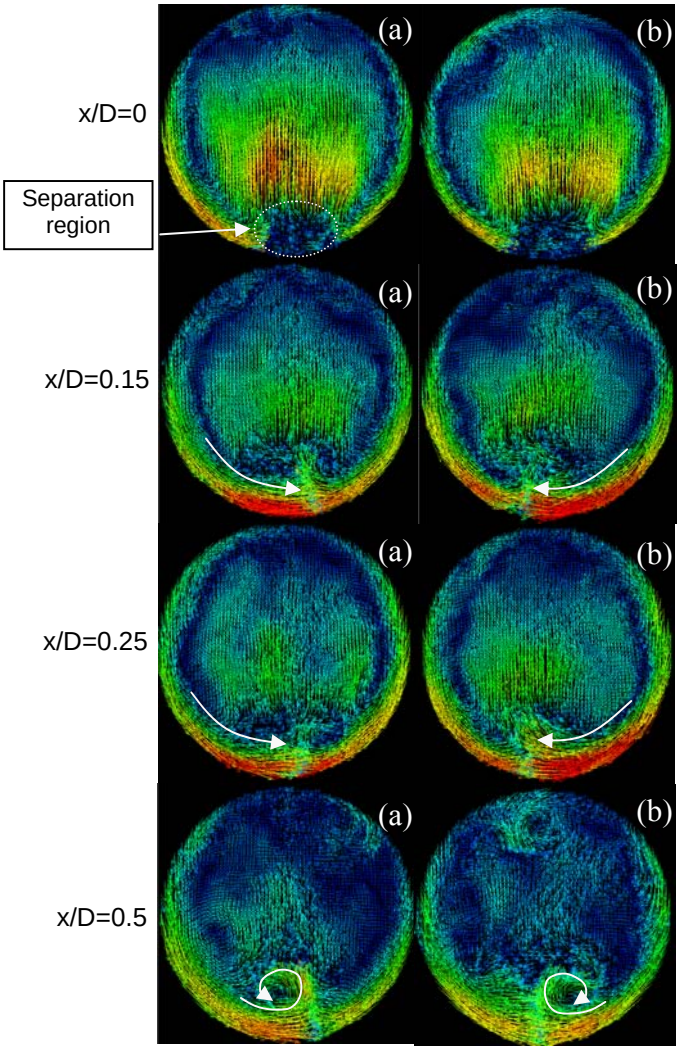

Figure 8 Instantaneous secondary flow in the cross-section at x/D=0, 0.15, 0.25 and 0.5 of the short-elbow.

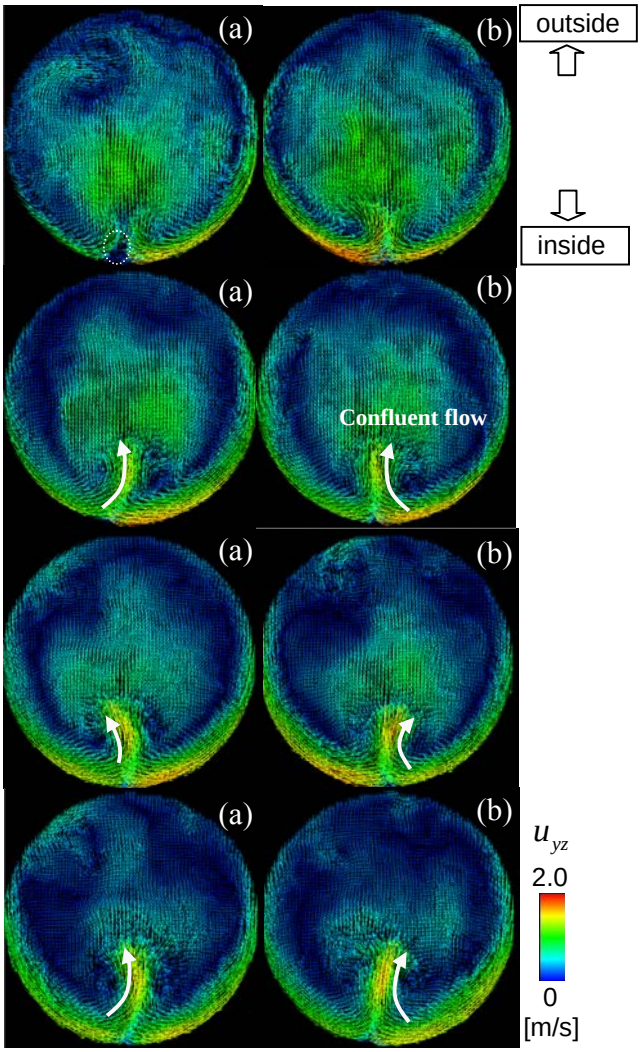

Figure 9 Instantaneous secondary flow in the cross-section at x/D=0, 0.15, 0.25 and 0.5 of the long-elbow.

flowed toward the separation region from both right and left. The accelerated flow for axial direction in the separation region as shown in Fig.6-(b) would be caused by the inflow of such circumferential secondary flows. In the cross-section of x/D=0.5, the circumferential secondary flows became weak. The vortexes in clockwise and counterclockwise direction were formed by the inflow of the circumferential secondary flow from a lateral wall.

Figure 9 shows the arbitrary instantaneous secondary flows in the cross-sections at x/D=0, 0.15, 0.25 and 0.5 in the long-elbow. At the cross-section of x/D=0 (a), the narrow separation region was formed at θ =180^o in the elbow. On the other hand, in another moment, x/D=0 (b), the narrow separation region was not formed. At the cross-section, the circumferential secondary flow in the long-elbow was weaker than that in the short-elbow. The circumferential secondary flows from both right and left sides met at θ =180^o and made high velocity flow toward the center of the pipe as shown by the white arrows. As shown in Fig.9, the flow direction of the confluent flow fluctuated from side to side. It seems that the 'medium velocity region' shown in Fig.7 could be formed by this confluent flow in radial direction. This confluent went in axial direction and toward the center of the pipe.

Figure10 shows the instantaneous velocity fields on an x-z plane at the short-elbow outlet near the elbow inside wall (y/D=0.08) at two different time stamps with different flow patterns. In Fig.10, the blue area where lower velocities were measured was the separation region. Combination of the Fig.10 and Fig.8 (the cross-section of x/D=0.15 and x/D=0.25) showed that the circumferential secondary flows flowed into the separation region as shown by the white arrows in Fig. 10 and Fig.8. The separation region fluctuated in transverse direction because of the alternative inflows of circumferential secondary flows as indicated by white arrows. It was also observed that the reverse flow flowed in the separation region. This reverse flow was seemed to be caused by inflow of circumferential secondary flow into the separation region, especially x/D=0.15. The separation region changed the shape from (a) to (b) or from (b) to (a). Figure 11 shows velocity field on the x-z plane in the long-elbow. In Fig.11, the narrow region along θ =180^o, where the flow velocity is low, corresponds to separation region. As is the case with the short-elbow, the secondary flows flowed toward 180^o line from both sides as shown by the white arrows. The motion of the separation region was less than that in the short-elbow since the circumferential secondary flows from both lateral sides relatively stable as shown in Fig.9.

Figure 12 shows the power spectrum density (PSD) of velocity fluctuation at θ =180^o, x/D=0.25 (the red point in Figs.10 and 11). The horizontal axis was Strouhal number, St=f・D/U_m. Here, f is the frequency, D is the pipe diameter, and U_m is the mean velocity. Since a prominent peak at St=0.57 was observed in the short-elbow, it is confirmed that the separation region near the inside wall of the elbow fluctuated periodically. In the long-elbow, the small peak was also found at St=0.65. Therefore, the flow near the inside wall of the elbow also fluctuated weakly but periodically. Kawamura et al. [9] reported that St numbers of prominent peaks distributed around 0.5 in the cases of r/D=0.55, 1 and 2. Our experimental results agreed with this finding of Kawamura el al. The slight scattering of these St numbers of prominent peaks would come from the difference of the size and shape of separation region.

From all of above experimental results, the flow structures in the short-elbow and the long-elbow are summarized as follows; in the short-elbow, the higher velocity at ϕ=30° due to the larger elbow curvature ratio forms the steep negative pressure gradient along the inside wall of the elbow. Therefore, the flow separation with the shape of 'bubble' occurs in midstream of curvature in the short-elbow. The separation region in the short-elbow interacts with the circumferential secondary flows and fluctuates in transverse direction periodically. On the other hand, the maximum velocity in the long-elbow is lower than that in the short-elbow since the curvature of long-elbow is smaller than that of the short-elbow. This result in the smaller negative pressure gradient along the inside wall of the long-elbow than that in the short-elbow. Therefore, the separation region formed in the long-elbow was narrow. In the long-elbow, the circumferential secondary flows coming from both lateral sides collide with each other above the narrow separation region and turn the direction to the center of the pipe. This radial flow is thin in azimuthal direction but long in axial direction like a sheet.

It was found that the flow structure including flow separation and secondary flow are greatly

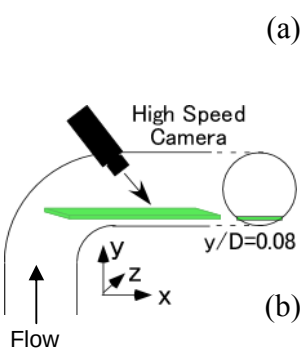

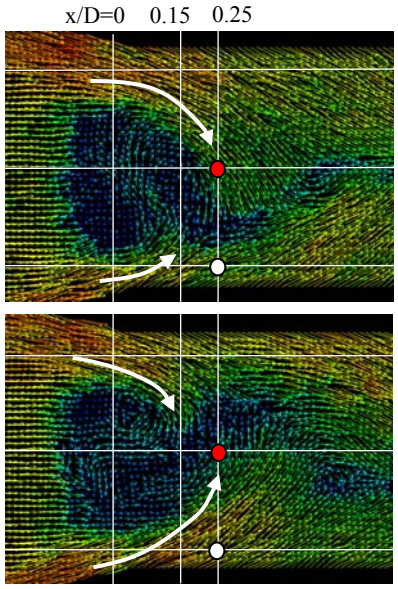

Figure 10 Instantaneous velocity field in the horizontal cross-section of the short-elbow near the inside wall.

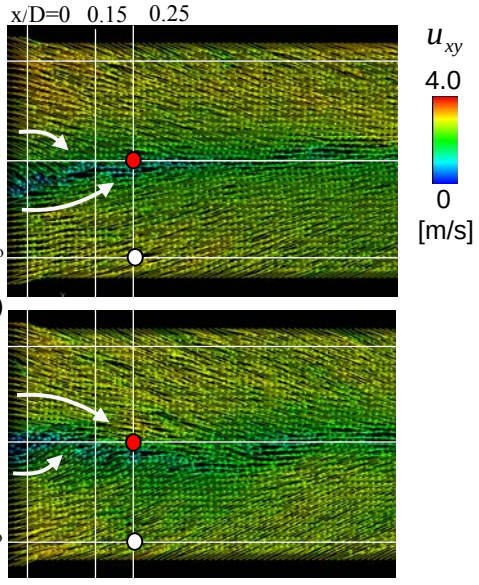

Figure 11 Instantaneous velocity field in the horizontal cross-section of the long-elbow near the inside wall.

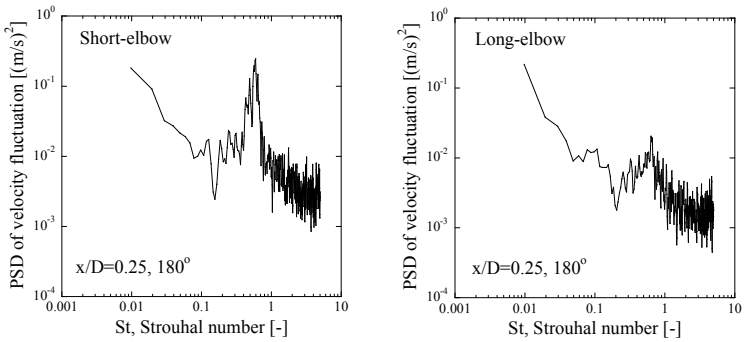

Figure 12 Power spectrum density of velocity at x/D=0.25 and 180° in the short-elbow and the long-elbow.

affected by the elbow curvature. In the next section, the relation between the pressure fluctuation and the flow structure is discussed in the short-elbow and long-elbow.

3.2 Pressure fluctuation in the elbow

Figure 13 shows time trend of the pressure fluctuation at each measurement point in the short-elbow. According to Figs.5 and 10, the measurement point of '0D-180°' was in the separation region. At the measurement point '0D-180°', some negative pressure spikes were observed. Shiraishi et al. [10-11] also observed similar negative pressure spikes in the pressure fluctuation signals downstream of the elbow outlet at circumferential angle θ =180° in the separation region. There were no fluctuations in positive pressure side since the separation region (the low pressure region) would stay on the '0D-180°' at all time. At the measurement point '0D-210°', the circumferential secondary flows flowed along the separation region. At the measurement point of '0D-210°', the negative spike was not observed and fluctuating pressure with positive and negative side were observed. It was found from Fig.10 that the cross-section of x/D=0.25 was the region that velocity fluctuated intensely due to the transverse motion of separation region and the inflow of circumferential secondary flow. At the measurement point '0.25D-180°', the negative spike and the pressure fluctuation with large amplitude were observed. This pressure fluctuation with large amplitude would be caused by the slide motion of separation region. The pressure fluctuation with large amplitude was observed also at measurement point '0.25D-210°' apart from '0.25D-180°'. Fig.10 showed that the boundary of separation region slid to around the circumferential angle of 210°.

Figure 14 shows the pressure fluctuations at each measurement point in the long-elbow. The amplitudes of the fluctuation pressures at all measurement points in the long-elbow were much smaller than those in the short-elbow. As shown in Fig.11, the measurement points of '0D-180°' and '0.25D-180°' were in the narrow separation region. On the other hand, the measurements points of '0D-210°' and '0.25D-210°' were outside of the narrow separation region. The pressure fluctuations on the 180° line in the separation region were greater than that on the 210° line outside of the separation region.

Figure 15 shows the power spectrum density of fluctuating pressure at the measurement point of '0D-210°' in the short-elbow and the long-elbow. The horizontal axis is Strouhal number, St. In both the short-elbow and the long-elbow, the power decreased with increasing in St number. This indicates the characteristics of turbulent flow. In the short-elbow, there was the distinct peak at St of 0.56. It was found that the periodic pressure fluctuation occurred at the short-elbow outlet. St number of 0.56 at the peak was close to that of velocity fluctuation at x/D=0.25 (See Fig.12). Therefore, the pressure fluctuation of St number of 0.56 is caused by the unsteady flow structure including the separation region and circumferential secondary flow. In the long-elbow, the power of pressure fluctuation in the long-elbow was smaller than that in the short-elbow and was not observed the distinct peak (the peak around St=0.14 was caused by inlet condition). Although the velocity fluctuations were periodic with St=0.57 and 0.65 in the short-elbow and the long-elbow respectively, the distinct peak of pressure fluctuation was not observed in the long-elbow. It was seemed that the pressure fluctuation with large amplitude in the short-elbow was caused by the slide motion of the large separation region like a bubble shape

(the low pressure region) which moved to right and left with time. Therefore, it was found that the cause of significant pressure fluctuation in the elbow was existence of the large separation region.

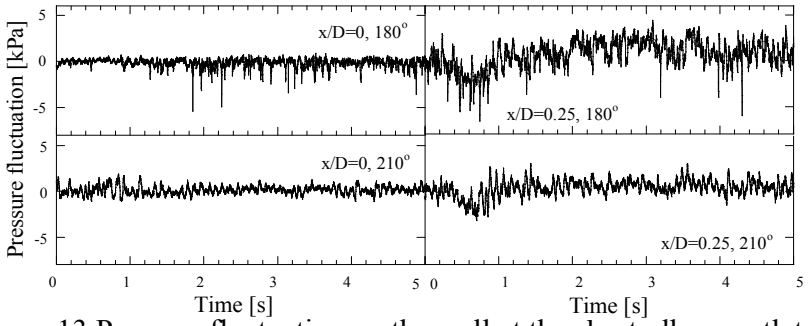

Figure 13 Pressure fluctuation on the wall at the short-elbow outlet.

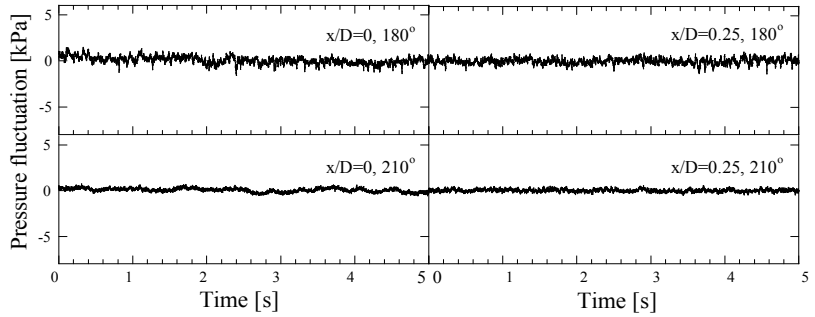

Figure 14 Pressure fluctuation on the wall at the long-elbow outlet.

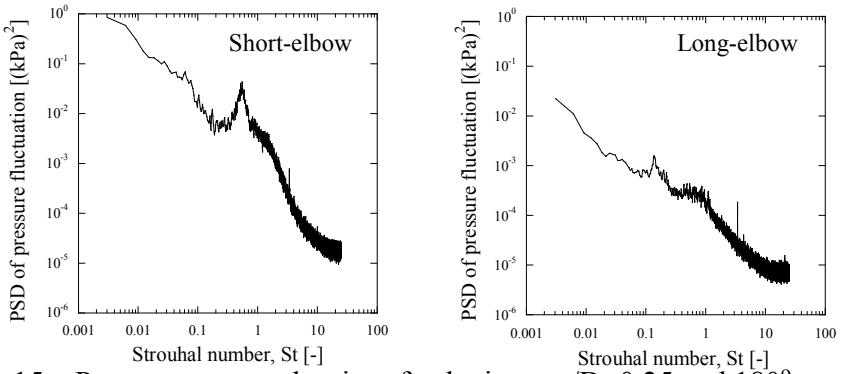

Figure 15 Power spectrum density of velocity at x/D=0.25 and 180° in the short-elbow and the long-elbow.

4. Conclusion

The water experiments of flow, which were 1/8 scaled down from the JSFR H/L pipe, were conducted for the different curvature ratio, r/D=1.0 and 1.5. The velocity fields in the elbow and pressure fluctuation on the inside wall of the elbow were measured at $Re=5.4x10^5$. The conclusions obtained in this study are summarized as follows;

(1) The flow structure in flow separation region near the inside wall of the elbow different between r/D=1.0 and r/D=1.5.

(2) The axial velocity fluctuations around the inside wall have dominant frequency at St=0.57 and 0.65 in the short-elbow and the long-elbow, respectively.

(3) In the short-elbow, the pressure on the inside wall fluctuated periodically with St=0.56. This frequency agreed nearly with the frequency of velocity fluctuation near the separation region. On the other hand, the significant pressure fluctuation was not observed on the inside wall of the long-elbow.

(4) The significant pressure fluctuation on the inside wall of the elbow was caused by sliding mortion the large separation region of bubble shape.

5. References

[1] Ichimiya, M., Mizuno, T. and Kotake, S., "A Next Generation Sodium-Cooled Fast Reactor Concept and Its R&D Program", J. Nuclear Engineering and Technology, 39, pp.171-186 (2007).

[2] Aoto, K., Uto, N., Sakamoto, Y., Ito, T., Toda, M. and Kotake, S., "Design Study and R&D Progress on Japan Sodium-Cooled Fast Reactor", J. Nuclear Science and Technology, Vol.48, No.4, pp.463-471 (2011).

[3] Dean, R. B., "Reynolds number dependence of skin friction and other bulk flow variables in two-dimensional Rectangular duct flow", J. fluids engineering, Vol.100, pp.215-223. (1978)

[4] Taylor, A. M. K. P., Whitelaw, J. H. and Yianneskis, M., "Curved duct with strong secondary motion velocity measurements of developing laminar and turbulent flow", J. fluids engineering, vol.104, pp.350-359 (1982).

[5] Crawford, N. M., Cunningham and Spedding, P. L., "An experimental investigation into the pressure drop for turbulent flow in 90^o elbow bends", J. Process Mechanical Engineering, Vol.221, part E, pp.77-88 (2007).

[6] Bovendeerd, P., Steenhoven, A., Vosse, F. and Vossers, G., "Study entry flow in a curvature pipe", J. Fluid Mech., 177, pp.233-246 (1987).

[7] Enayet, M. M., Gibson, M. M., Taylor, A. M. K. P. and Yianneskis, M., "Laser-Doppler measurements of laminar and turbulent flow in a pipe bend", Int. J. Heat and Fluid Flow, 3, No.4, pp.213-219 (1982).

[8] Sudou, K. and Hibara, H., "Turbulent Flow in a Circular-Sectioned 90^o Bend", Trans. Jpn. Soc. Mech. Eng. B, 58, 548, pp.1015-1021 (1992).

[9] Kawamura, T., Nakao, T. and Takahashi, M., "Reynolds Number Effect on Turbulence downstream from Elbow Pipe", Trans. Jpn. Soc. Mech. Eng. B, 68, 677, pp.645-651 (2001).

[10] Shiraishi, T., Watakabe, H., Sago, H., Konomura, M., Yamaguchi, A. and Fujii, T., "Resistance and Fluctuating Pressure of a Large Elbow in High Reynolds Numbers", J. of Fluids Engineering, 128, pp.1063-1073 (2006).

[11] Shiraishi, T., Watakabe, H., Sago, H., Kotake, S. and Yamano, H., "Pressure Fluctuation Characteristics of the Short-Radius Elbow Pipe for FBR in the Postcritical Reynolds Regime", Proc. of Int. Conf. on Jets, Wakes and Separated Flows, ICJWSF-2008, Berlin, Germany (2008).

[12] Ono, A., Kimura, N., Kamide, H. and Tobita, A., "Study on Flow-Induced Vibration Evaluation of Large-Diameter Pipings in a Sodium-Cooled Fast Reactor –Study on Unsteady Flow Structure and Characteristics of Pressure Fluctuation-", Proc. of the 7th Korea-Japan Symp. On Nuclear Thermal Hydraulics and Safety, Chuncheon, Korea (2010).

[13] Sakakibara, J., Hishida, K. and Maeda, M., "Simultaneous measurements of two dimensional velocity and temperature field using correlation technique and LIF, flow visualization VI", Proc. of the 6th Int. Symp. on Flow Visualization, Springer-Verlag, pp.677-681 (1992).

[14] Idelchik, I. E., "Handbook of Hydraulic Resistance", Second Edition, Hemisphere Publishing Co., pp.271-275, (1986).